INVERSE PROBLEM FOR DETERMINATION OF THE BUBBLE SIZE SPECTRUM

ANNA BARANOWSKA, ZYGMUNT KLUSEK

Institute of Oceanology, Polish Academy of Sciences
Powstańców Warszawy 55, 81-712 Sopot, Poland
anbar@iopan.gda.pl

The aim of this paper is a presentation of problems that might arise during determination of the bubble size spectrum in the sea using an inverse acoustics method. The mathematical model is introduced and limits of its numerical solution are discussed. Theoretical considerations lead to ill-posed system of integral equations and the system of linear equations resulting from a discretization process is solved using the Tikhonov regularization method. A mathematical model is tested for a power-law bubble size distribution. Some examples of theoretical studies related to this problem are provided. Practical applications of the bubble population determination algorithm on the basis of collected in situ empirical data concerning sound speed and attenuation are given.

INTRODUCTION

Gas bubbles in the ocean are generated by breaking waves, biological activity, ships and other various mechanisms. Both single bubbles and bubble clouds in the water body could be observed and counted with acoustic methods. Knowledge of the bubble size spectrum is very important in oceanography. Existence of bubbles in water plays an important role in the processes of generation, absorption and scattering of underwater sound. Moreover, moving bubbles constitute efficient source of the ambient noise in the ocean. In fact, diverse factors such as the wind speed, water temperature, depth and others have influence on the bubble concentrations and size distribution.

Different techniques are employed for bubbles sizing. For some classes of measurements inverse methods or iterative inverse bubble sizing techniques are required. Subsequently, it is possible to find the bubble density spectrum functions. It is also important to remember that these methods have many limitations. For example, they are not suitable in the case of high value of the gas void fraction. Simultaneously with experiments, theoretical and numerical studies are conducted. During theoretical investigations many authors use simple bubble distributions such as single-size, Gaussian or power-law functions.

Knowledge of the bubble size spectrum allows calculating the sound speed and attenuation in bubbly water. In this paper inverse problem is considered. We assume that the sound speed and attenuation are measured and the bubble size spectrum can be determined on the basis of these parameters. The paper presents theoretical considerations of the bubble size spectrum calculations and gives some information about methods of the sound speed and attenuation measurements.

1. GOVERNING EQUATIONS

We consider a bubbly liquid with bubbles of radii from a_L to a_U meters. The square of the complex wave number κ we write using the Commander and Prosperetti formula [2]:

$$\kappa^2 = k^2 + 4\pi \int_{a_L}^{a_U} \frac{n(a)a}{\omega_0^2/\omega^2 - 1 + i\delta_t} da \tag{1}$$

where $k = \omega/c_0$ is the acoustic wave number, $\omega = 2\pi f$ is the angular frequency and c_0 is sound speed in pure liquid, δ_t is the damping coefficient, ω_0 is the resonance angular frequency of a bubble, $n(a)$ is the number of bubbles per unit volume with radii a in $da = 1\mu$m range.

The resonance angular frequency ω_0 of a bubble with radius a can be determined using the formula [1]:

$$\omega_0^2 = \frac{p_0}{\rho_0 a^2}\left(\mathrm{Re}\,\Phi - \frac{2\sigma}{p_0 a}\right) \tag{2}$$

with

$$\Phi = \frac{3\gamma}{1 - 3(\gamma-1)\, i\, z[(i/z)^{1/2}\coth(i/z)^{1/2} - 1]} \tag{3}$$

where $z = D/(\omega a^2)$ and D is the gas thermal diffusivity, ρ_0 is the density in pure liquid. The quantity p_0 is the undisturbed pressure in the bubble and is given by $p_0 = P_0 + 2\sigma/a$, where P_0 denotes the equilibrium pressure in the liquid. The damping coefficient δ_t is the sum of the viscous damping constant, the damping constant due to thermal effects and the acoustic radiation damping constant:

$$\delta_t = \frac{4\mu}{\rho_0 \omega a^2} + \frac{p_0}{\rho_0 a^2 \omega^2}\mathrm{Im}\,\Phi + \frac{\omega a}{c_0} \tag{4}$$

where μ is the coefficient of molecular viscosity of seawater.

Setting

$$\frac{\kappa}{k} = u - iv \tag{5}$$

and separating the real and imaginary parts in Eq. (1) after some calculations we obtain two new equations [3, 5]:

$$\frac{4\pi}{k^2}\int_{a_L}^{a_U}\frac{\left(\omega_0^2/\omega^2-1\right)a}{\left(\omega_0^2/\omega^2-1\right)^2+\delta_t^2}n(a)da=\int_{a_L}^{a_U}K_1(a,\omega)n(a)da=u^2-v^2-1, \tag{6}$$

$$\frac{2\pi}{k^2}\int_{a_L}^{a_U}\frac{\delta_t\, a}{\left(\omega_0^2/\omega^2-1\right)^2+\delta_t^2}n(a)da=\int_{a_L}^{a_U}K_2(a,\omega)n(a)da=uv. \tag{7}$$

Finally we obtain the Fredholm integral equations of the first kind:

$$\int_{a_L}^{a_U}K(a,\omega)n(a)da=g(\omega). \tag{8}$$

Figure 1 shows the kernel functions $|K_1|$ and K_2 as a function of the bubble radius for different frequencies. Function K_1 is positive for radii less than the resonant radius, zero at this radius and negative for larger radii. Function K_2 is peaked at resonant radius and positive for all radii.

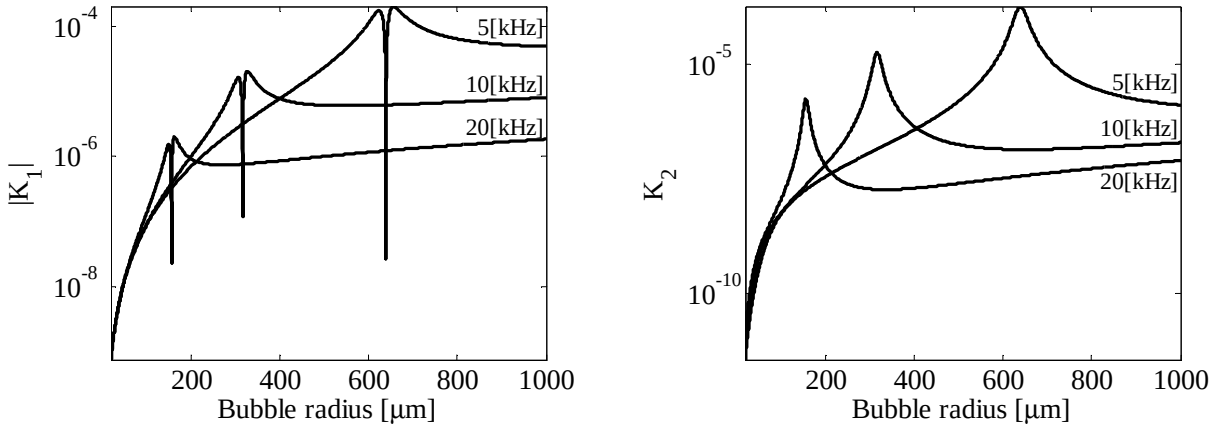

Fig.1. The kernel functions $|K_1|$ and K_2 versus the bubble radius for different frequencies.

The quantity u and v we can compute by measuring the phase velocity C in m/s and the attenuation α in dB/m. The relationship between these values is follows:

$$C=c_0/u, \quad \alpha=20\log_{10}e\frac{\omega v}{c_0}. \tag{9}$$

To verify the proposed numerical model the sound speed and attenuation were calculated using Eq. (1). Numerical investigations were carried out for the bubble population density $n(a)=n_0a^{-3}$ where n_0 is constant calculated using assumed value of the volume fraction β given by

$$\beta=\frac{4\pi}{3}\int_{a_L}^{a_U}a^3n(a)da. \tag{10}$$

2. INVERSE PROBLEM

To solve numerically Eq. (8) we divide the interval $[a_L, a_U]$ into M subdomains and write this equation in the form

$$\sum_{j=1}^{M} \int_{a_j}^{a_{j+1}} K(a_j, \omega) n(a_j) da = g(\omega). \tag{11}$$

Two different methods of discretization of Eq. (11) are used. First of them depends on linear interpolation of the unknown function n inside each interval $[a_j, a_{j+1}]$ in the following way [3]:

$$n(a) = N_j \frac{a - a_{j+1}}{a_j - a_{j+1}} + N_{j+1} \frac{a - a_j}{a_{j+1} - a_j} \tag{12}$$

where $N_j = n(a_j),\ j = 1, 2, ..., M+1$. Substituting above functions into Eq. (11) we obtain:

$$\sum_{j=1}^{M} \int_{a_j}^{a_{j+1}} K(a_j, \omega) \left[N_j \frac{a - a_{j+1}}{a_j - a_{j+1}} + N_{j+1} \frac{a - a_j}{a_{j+1} - a_j} \right] da = g(\omega). \tag{13}$$

Another approximation of Eq. (11) proposed by the author has the form:

$$\sum_{j=1}^{M} \left[K(a_j, \omega) N_j + K(a_{j+1}, \omega) N_{j+1} \right] \frac{a_{j+1} - a_j}{2} = g(\omega). \tag{14}$$

If we know the values of function g for frequencies $\omega_i,\ i = 1, 2, ..., N$, we can write N linear equations and, in consequence, the system of linear equations

$$\boldsymbol{KN} = \boldsymbol{g}. \tag{15}$$

The integrals in matrix $\boldsymbol{K}$ must be calculated numerically and the values of vector $\boldsymbol{g}$ are calculated using measured values of phase speed and attenuation.

The kernel function K in Eq. (8) is analytic and compact and in consequence of this fact the equation is ill-posed. To solve system (15) the Tikhonov regularization is used:

$$(\boldsymbol{K}^T \boldsymbol{K} + \varepsilon \boldsymbol{I}) \boldsymbol{N} = \boldsymbol{K}^T \boldsymbol{g} \tag{16}$$

where $\boldsymbol{K}^T$ is the transpose of matrix $\boldsymbol{K}$, $\boldsymbol{I}$ is the identity matrix and ε is a regularization parameter .

3. RESULTS OF NUMERICAL INVESTIGATIONS

Numerical calculations were carried out for different values of frequencies and the bubble radius range. Firstly, we assumed that the bubble radii were from 20 μm to 320 μm and frequencies change from 5 kHz to 155 kHz. The values of the regularization parameter

we experimented with ranged from 10^{-35} to 10^{-20}. Figure 2 presents inverse problem solution obtained for two different values of this parameter. The dashed line represents the exact solution and the solid line depicts numerically obtained bubble density distribution. An exact analysis shows that in this situation it is impossible to obtain solution with the relative error less than 10% for all investigated bubble radii. However, it is possible to obtain such a solution in subintervals [20 µm, 150 µm] or [150 µm, 320 µm] correspondingly.

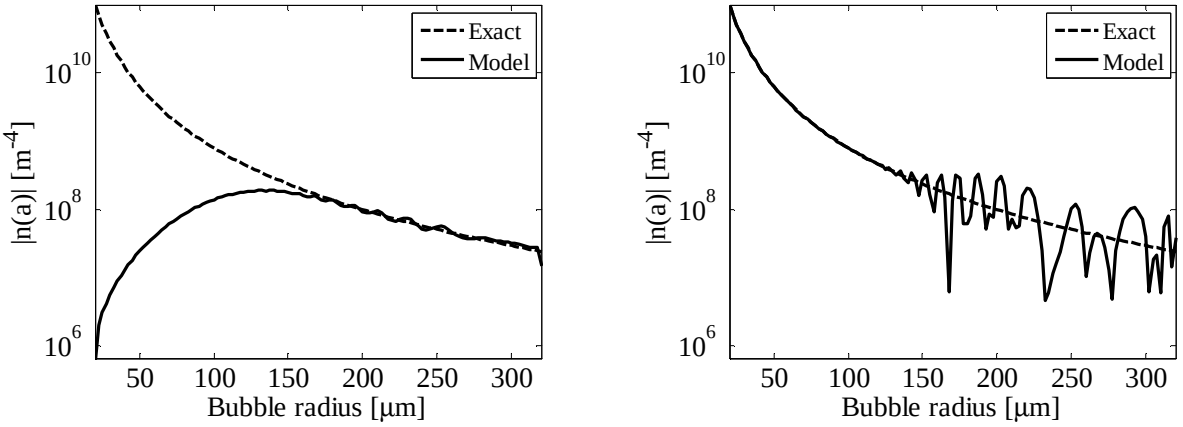

Fig.2. Inverse problem solution for different values of the regularization parameter: bubble radius from 20 µm to 320 µm and frequency from 5 kHz to 155 kHz.

Other results we obtain when frequency changes from 2 kHz to 22 kHz and the bubble radius interval is the same as in the previous case. Figure 3 shows inverse problem solutions for this situation and different values of ε parameter. Now it is possible to obtain the results with the relative error less than 10% only for bubble radii from 120 µm to 250 µm.

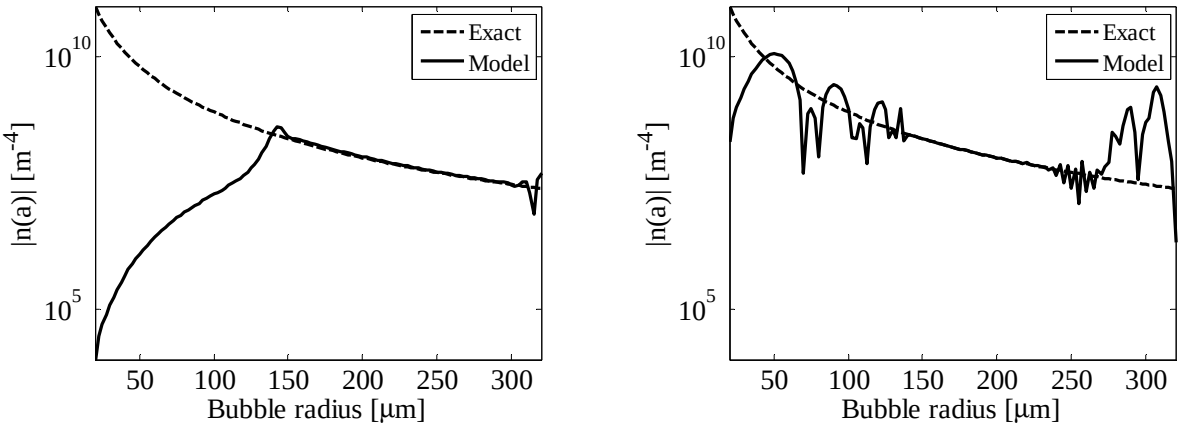

Fig.3. Inverse problem solution for different values of the regularization parameter: bubble radius from 20 µm to 320 µm and frequency from 2 kHz to 22 kHz.

The next figure shows results obtained for the same values of frequencies i.e. from 2 kHz to 22 kHz as earlier and for the bubbles from 160 µm to 300 µm. In this situation, we found solution where the relative error is less than 10% for all bubbles.

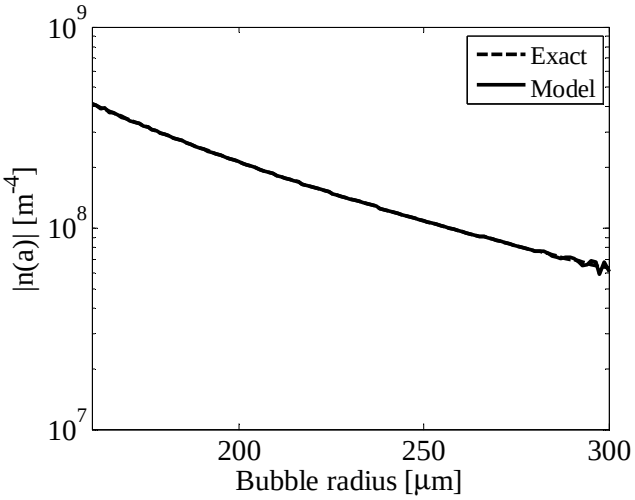

Fig.4. Inverse problem solution for different values of the regularization parameter: bubble radius from 160 μm to 300 μm and frequency from 2 kHz to 22 kHz.

An exact analysis shows that it is impossible to choose correct value of the regularization parameter before starting numerical calculations. To analyze this problem more carefully we collected the results of numerical calculations obtained for different values of this parameter. Figure 5 depicts the results of numerical calculations (marked by stars) for frequencies changing from 2 kHz to 22 kHz and different intervals of bubble radius. We took the values of the regularization parameter varying from 10^{-35} to 10^{-20}. The left figure presents that case for bubbles from 20 μm to 320 μm, however we cannot obtain correct solution for bubble radii smaller than 50 μm. When the bubble radius changes from 160 μm to 300 μm (the right figure) then the solution of the inverse problem is different. This time we obtain different solutions for different values of parameter ε and it is possible to choose such a value of this parameter that the solution is exact for all radii.

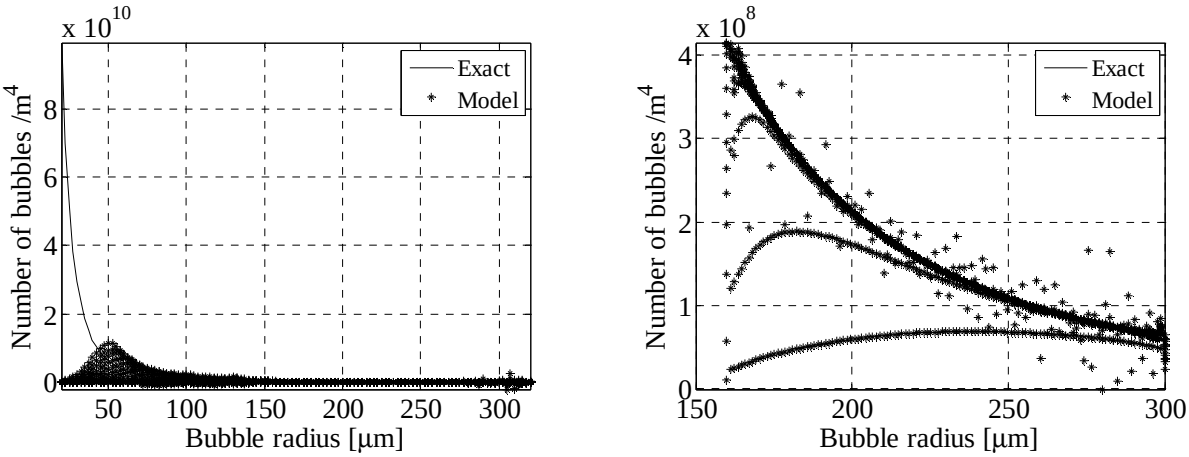

Fig.5. Inverse problem solution for different values of the regularization parameter: bubble radius from 20 μm to 320 μm (left) and from 160 μm to 300 μm (right).

As it is obviously observed in Fig. 5, an ill-posed problem may have more than one solution or do not have any solution. But this property is not the only one difficulty which

characterizes such problems. In addition to this the solution may not depend continuously on the initial data. Figure 6 describes solution of the third example (Fig. 4) when randomly selected data errors of function *g* were less than 10% in each point.

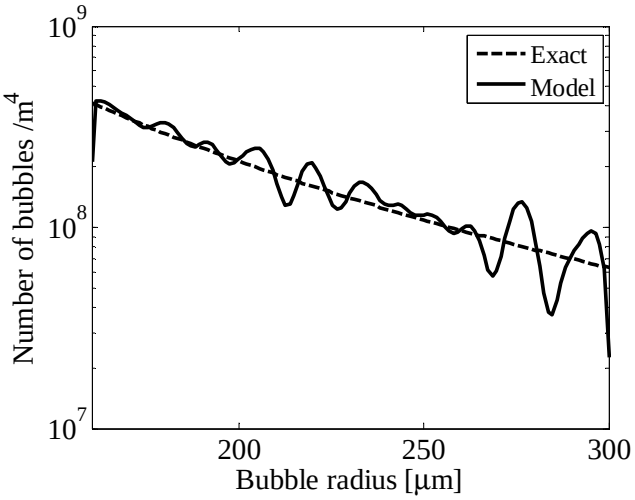

Fig.6. Inverse problem solution with randomly selected data errors.

All the results of numerical calculations presented in this paper we carried out using Eq. (13). Usually we obtain better accuracy using this model but it is not a rule. It is worth noticing that the second model (Eq. (14)) has important advantages. Because there is not any numerical integration during calculations, it is easier to write a computer program for this model and it works faster. The inverse problem requires many different calculations therefore the second model can be more useful especially during initial numerical tests.

4. SOUND SPEED AND ATTENUATION DETERMINATION

During numerical tests we have chosen the frequencies, the bubble radii and additionally we have assumed that the bubble size spectrum is known. On the basis of these data the matrix $\boldsymbol{K}$ and vector $\boldsymbol{g}$ were calculated. In practice, the matrix $\boldsymbol{K}$ is determined in the same way but vector $\boldsymbol{g}$ is work out using sound speed and attenuation obtained from experimental data.

The input data to the presented above theoretical mode, the method of the measurements of the phase sound speed and attenuation proposed by Terrill and Melville [4] was tested in experiments carried out at sea. In the experiments, a broadband pulses in the form of chirps with linear or with quadratic instantaneous frequency deviation were transmitted. The frequencies of transmitted signals were from 2 kHz to 20 or up to 25 kHz, the pulses duration was 10 or 15 ms. Signal was transmitted by the Soviet hydrophone G005 (with removed preamplifier), and as receiver the calibrated hydrophone Brüel&Kjær Type 8105 was employed. Signals were designed and formed with the A/D card NI 6351. As the signal power amplifier, driving the transmitter, the power amplifier L-2 Instruments Inc was employed. Synchronously, the same card was used as the signal sampler at the rate 120/130 kS/sec, with the resolution 16 bit. The A/D card control, signal design, reception and pre-processing were carried out in MATLAB environment. Signals were send in 100 ping series with repetition time between transmission 30 ms. However, the ping rate is limited by the communication speed between A/D card and the computer, and some ping records were missing. The distance

between transmitter and hydrophone was L=0.4 m, and the distance from the ship board greater than 3 m. Records were performed at the depth of 1 m. During measurements the sea state was 3B.

The frequency response of the Brüel&Kjær Type 8105 hydrophone is practically flat in the utilised frequency range. The transmit voltage response curve of the spherical of cylindrical transmitters are strongly dependent on frequency, with typical 6 – 7 dB/octave increasing with frequency, up to its resonance frequency (in original paper by Terrill and Melville, the frequency transmit voltage response of their transmitter was given incorrectly). Therefore, corresponding amplitude correction of the sending signals was applied. To test quality of received signals in the lower frequency range the nonlinear, up going quadratic frequency modulation was used.

The phase correction for both the transmitter, and receiver were not taken into account, in the post processing, as the less relevant in comparison with the effects of the signal distortions during propagation through bubble water.

The examples of the form of received chirp signals and their envelopes propagated through bubbly (upper panel) and bubble-free water are presented in Fig. 7.

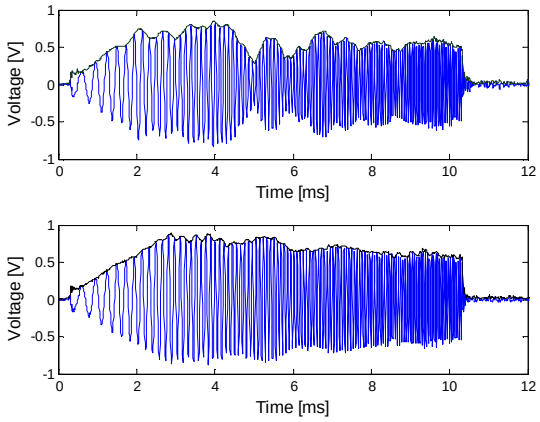

Fig.7. Examples of the forms of a received chirp signal in the case of disturbed (upper panel) and bubble-free water.

Envelopes of 100 pings, of received signal during sounding with the LFM signals where the vertical axis (the time) is proportional to instantaneous frequency between 2 and 20 kHz are presented in Fig. 8. In the image, a segment with higher signal attenuations is clearly visible between the 10th and 20th pings. The fluctuations of phase speed in all set of pings are also noticeable in the form resembles of a moiré pattern.

In the course of post processing the received signals were filtered in 20 equidistant frequency bands between 2 kHz and 20 kHz with the FFT inverse transform. The inverse FFT procedure is actually a two-step operation that applies a filter in the FFT domain with convolution with rectangular window and inverts the FFT image back to the original data space. Maxima of filtered time series were found and times of flight in each frequency band in relation to the time of the signal transmission in the same frequency range were computed.

Figure 9 presents time series of samples number for found maxima in the selected narrow frequency bands. Black curve represent maxima in filtered received signals, red line below samples of local maxima of signal at the output of A/D card. The phase sound speed in given frequency band $c(f)$ is estimated according to formula:

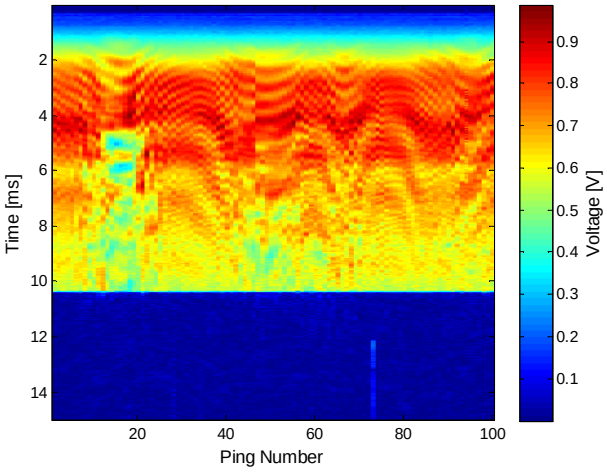

Fig.8. Signal envelopes of series 100 pings.

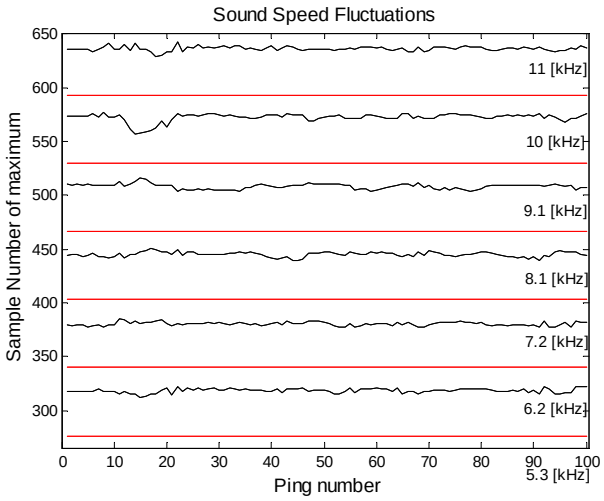

Fig.9. Time series of sample number of maxima in selected frequency bands.

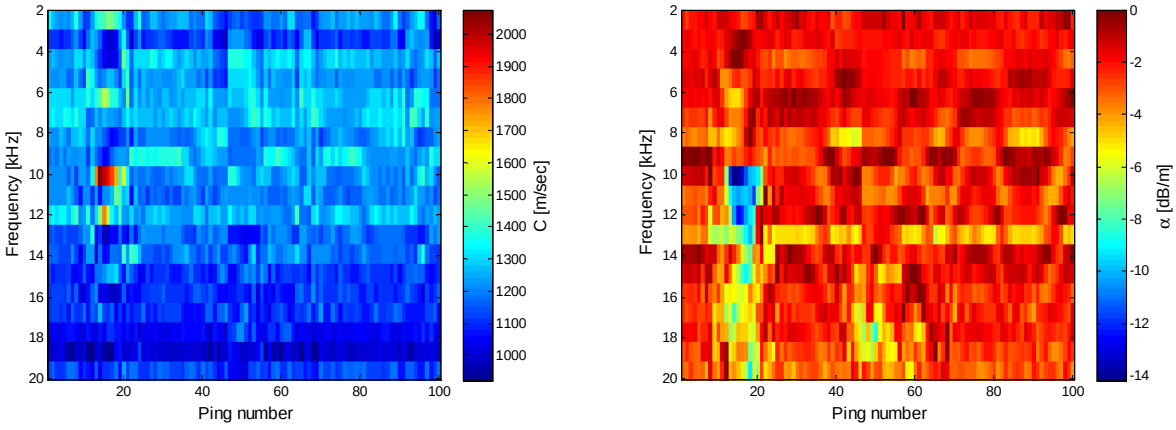

Fig.10. Phase sound speed and attenuation fluctuations at different frequencies during breaking event.

$$c(f) = L/\left[(n_{receiver} - n_{A/D}) \cdot dt\right] \tag{17}$$

where $n_{receiver}$ is sample number of maximum in given frequency band in received signal, and $n_{A/D}$ is sample number of maximum in given frequency band at A/D output.

Figure 10 shows the phase sound speed fluctuations and sound attenuation in frequency bands in the 100 consecutive pings.

5. CONCLUSIONS

The problem of the bubble sizes spectrum determination was considered. This problem was theoretically solved using methods suitable for inverse problems. Two different methods of discretization of the obtained Fredholm integral equation are presented. Usually we obtain better accuracy using the first of them but it is not a rule. The second discretization method has one important advantage. Using it there is no need for integration during calculations. It is worth to write here that we derived the Fredholm equation with two different kernels but during calculations only the second equation, i.e. Eq. (7) is generally used. To solve the obtained ill-posed problem the Tikhonov regularization was proposed. Calculations were carried out using own computer programs in MATLAB. The procedures were tested on analytical data assuming power-law bubble size distribution. Numerical investigation shows that it is impossible to choose value of the regularization parameter before starting numerical calculations. Moreover most often we find correct solution only in subintervals of bubble radii.

As an input data to the presented algorithm directly measured the sound speed and attenuation over a relative broad range of frequencies were tested. The possibility to measure at the same time both the real and imaginary parts of the complex dispersion relationship with simple setup looked at the beginning steps as very promising. However, numerical problems that arise due to specific properties of the theoretical model need more careful examinations. Another problem is the frequency dependence of transmitting voltage response of ceramic transducers, which requires a construction of special design of sounding signals and/or specialised power amplifiers.

ACKNOWLEDGEMENTS

The work has been supported by the grant nr 2011/03/B/ST10/05977 of the National Science Centre in Poland.

REFERENCES

[1] A. Baranowska, Numerical investigations of the nonlinear waves generation in a bubble layer, Hydroacoustics, Vol. 15, 7-12, 2012.

[2] K. W. Commander, A. Prosperetti, Linear pressure waves in bubbly liquids: Comparison between theory and experiments, J.Acoust.Soc.Am., Vol. 85 (2), 732-746, 1989.

[3] R. Duraiswami, S. Prabhukumar, G.L. Chahine, Bubble counting using an inverse acoustic scattering method, J. Acoust. Soc. Am. 104 (5), 2699-2717, 1998.

[4] E. J. Terrill, W. K. Melville, A broadband acoustic technique for measuring bubble size distributions: Laboratory and shallow water measurements, J. Atmos. Oceanic Technol., Vol. 17, 220–239, 2000.

[5] X. Wu , G. L. Chahine, Development of an acoustic instrument for bubble size distribution measurement, Journal of Hydrodynamics, Vol. 22(5), 325-331, 2010.